

Full Research Paper

Quantitative Boundary Support Characterization for Cantilever MEMS

Gino Rinaldi, Muthukumaran Packirisamy * and Ion Stiharu

Optical Microsystems Laboratory, CONCAVE Research Center Department of Mechanical & Industrial Engineering, Concordia University, Montreal H3G 1M8, Canada

E-mail: grin@alcor.concordai.ca; pmuthu@alcor.concordia.ca; istih@alcor.concordai.ca

* Author to whom correspondence should be addressed.

Received: 6 September 2007 / Accepted: 26 September 2007 / Published: 3 October 2007

Abstract: Microfabrication limitations are of concern especially for suspended Micro-Electro-Mechanical-Systems (MEMS) microstructures such as cantilevers. The static and dynamic qualities of such microscale devices are directly related to the invariant and variant properties of the microsystem. Among the invariant properties, microfabrication limitations can be quantified only after the fabrication of the device through testing. However, MEMS are batch fabricated in large numbers where individual testing is neither possible nor cost effective. Hence, a suitable test algorithm needs to be developed where the test results obtained for a few devices can be applied to the whole fabrication batch, and also to the foundry process in general. In this regard, this paper proposes a method to test MEMS cantilevers under variant electro-thermal influences in order to quantify the effective boundary support condition obtained for a foundry process. A non-contact optical sensing approach is employed for the dynamic testing. The Rayleigh-Ritz energy method using boundary characteristic orthogonal polynomials is employed for the modeling and theoretical analysis.

Keywords: MEMS, cantilevers, microfabrication, boundary support, Rayleigh-Ritz

1. Introduction

Boundary supported suspended microstructures, such as MEMS cantilevers, are currently used in various microengineering sensor/actuator fields. Their relatively simple geometries make them very

advantageous both from a design and microfabrication point of view. The wide range of applications include, for example, medical [1-6], optical [7-10], and microscopy [11-15], where the sensing mechanism depends upon the sensitivity or response of the cantilever to some applied excitation. In this regard, the mechanical characteristics of MEMS cantilevers, in general, depend upon the elastic properties of the microfabricated structures [16-18] resulting from the choice of material, geometry and operational environment, and the boundary support of the elastic structure [19].

Microfabrication methods and limitations can lead to boundary support conditions for suspended microstructures that are not rigidly clamped [20-25]. Hence, the boundary support condition needs to be theoretically quantified [16-18, 26, 27], and experimentally validated [28, 29]. In this regard, support boundary characterization is important in such applications such as flexible optical waveguides [30], and AFM cantilever probes [12], where a non-classical boundary support condition will significantly influence the static and dynamic behavior of the microstructure.

The term boundary conditioning refers to the integrated influences of material property, device geometry, boundary support, and operating conditions on the elastic characteristics of a suspended microstructure. This paper presents an experimental approach to quantify the support boundary condition of AFM cantilevers through electro-thermo-mechanical testing. To apply the proposed experimental method, the boundary support condition for AFM microcantilevers provided by MikroMasch [31] is investigated. The analytical formulation is based on the Rayleigh-Ritz energy method with boundary characteristic orthogonal polynomials [32]. In the Rayleigh-Ritz approach presented here, the support boundary and electrostatic influence are modeled by artificial springs [17, 18, 26, 27, 33].

A scanning electron microscope (SEM) image of three AFM cantilevers and a close up of the non-classical boundary support are illustrated in Figure 1. In Figure 1b L is the length of the cantilever and h is the thickness. Shown in Figure 2 is a side view of the cantilever and boundary support modeled with artificial translational K_T (N/m), and rotational K_R (N·m) springs, ξ is the positional coordinate along the length of the cantilever.

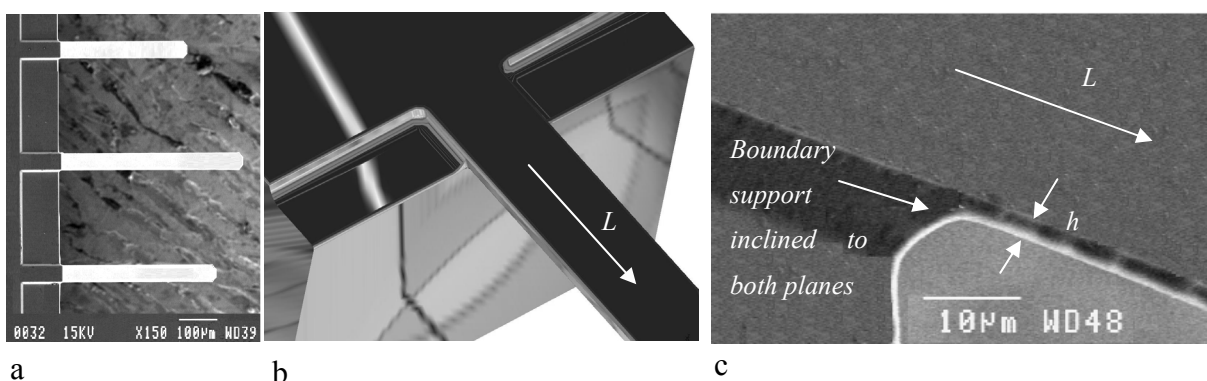


Figure 1. a) AFM chip with 3 microcantilevers. b) CAD drawing of a microcantilever boundary support. c) Close up image of the non-classical boundary support.

For the case of an electro-thermally actuated AFM probe, as shown in Figure 3, the electrostatic effect is represented by artificial electrostatic springs $k_E(x)$, where the total electrostatic stiffness is defined as, $K_E = \int_0^1 k_E(x) dx$, and where x is non-dimensionalized and equal to $\frac{\xi}{L}$ and ranging from 0 to

1.

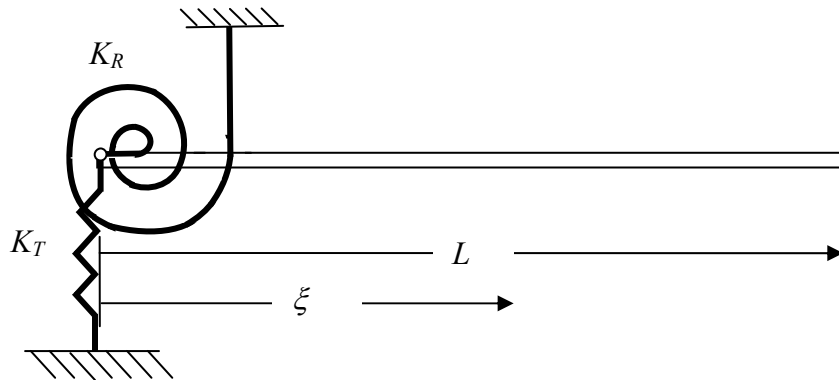


Figure 2. The non-classical boundary support modeled by artificial translational, K_T , and rotational K_R springs.

The thermal effect is modeled through changes in the cantilever geometry and material property [29, 33], also taking into account variations of Young's modulus of elasticity and coefficient of thermal expansion for single crystal silicon [34-39].

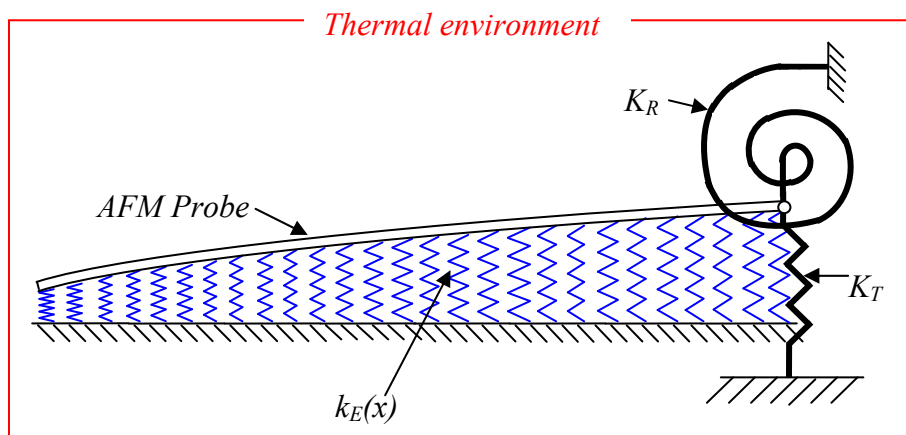


Figure 3. Environmental influences on an AFM cantilever modeled with artificial springs.

2. Results and Discussion

The dimensions, (L is the length, w is the width, h is the thickness) for the 12 AFM cantilevers, designated with G , tested in this work, where the $G1$ probe is tested under electro-thermo-mechanical influences are given in Table 1. The Young's modulus of elasticity E , and density ρ , are respectively,

169.5×10^9 Pa and 2330 kgm^{-3} for all of the probes tested. The dimensions presented are average values for a given cantilever and were measured using SEM and optical microscope images.

Table 1. The geometry of the 12 cantilevers tested in this work.
The geometrical dimensions are in micrometers.

<i>G</i>	<i>1</i>	<i>2</i>	<i>3</i>	<i>4</i>	<i>5</i>	<i>6</i>	<i>7</i>	<i>8</i>	<i>9</i>	<i>10</i>	<i>11</i>	<i>12</i>
<i>L</i>	351	299	254	251	251	300	302	353	250	302	304	355
<i>w</i>	35	35	36	35	35	36	35	36	36	35	36	36
<i>h</i>	0.95	0.96	0.93	0.92	1.00	1.05	1.10	0.94	0.90	0.94	1.93	1.89

Given in Figure 4 are the mapped experimental resonant frequencies at different applied DC voltages and temperatures for the *G1* probe.

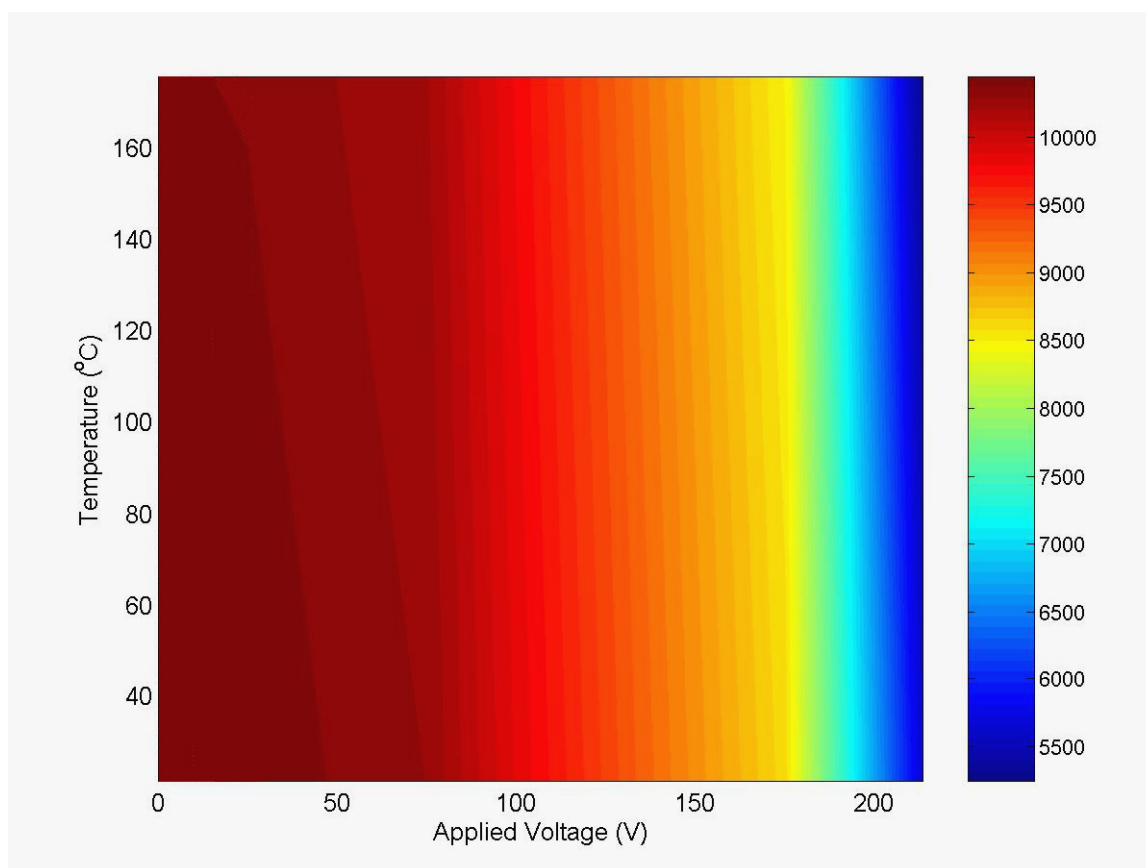


Figure 4. Resonant frequency map obtained for the *G1* AFM cantilever as a function of the temperature and applied DC voltage.

The non-linear experimental and non-classical boundary support resonant frequency variations, at different temperatures, as a function of the applied DC voltage for the *G1* cantilever are shown in Figure 5. The results are presented in tabular form in Table 2.

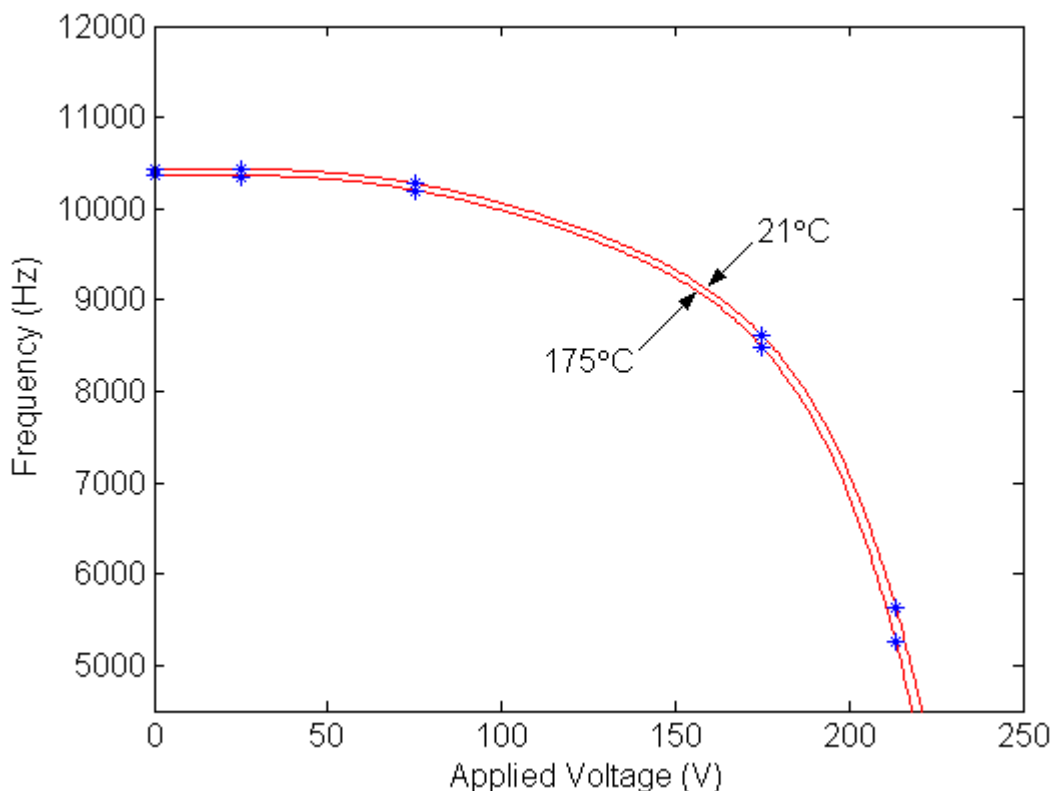


Figure 5. The resonant frequencies, at different temperatures, of the *GI* AFM cantilever as a function of the applied DC voltage. The solid lines are the non-classical boundary support models. The standard deviations are 34.86 and 35.35 Hz for 21°C and 175°C, respectively.

From the results obtained it can be clearly seen that there is a non-classical boundary support condition present due to the limitations of the microfabrication process. In this regard, for these two test methods on the *GI* AFM cantilever, an invariant rotational stiffness K_R^* (non-dimensional) values ranging from 108 to 109.5 as shown in Figure 6b were obtained as a function of the thermal loading. Shown in Figure 6a is the dependence of the AFM cantilever's length L , Young's modulus of elasticity E and moment of inertia I , on temperature. From the plotted values given in Figure 6a it can clearly be seen how sensitive Young's modulus of single crystal silicon is to temperature, and how its amplitude changes much faster than the other two parameters given. Electrostatic fringe effects were not considered in the model as they were found to be negligible (the K_R^* values obtained at 0V remained unchanged at the various temperatures). Also, the amplitude of the sinusoidal AC base excitation was small enough so that its contribution to the total electrostatic stiffness K_E was negligible but large enough to obtain a frequency response.

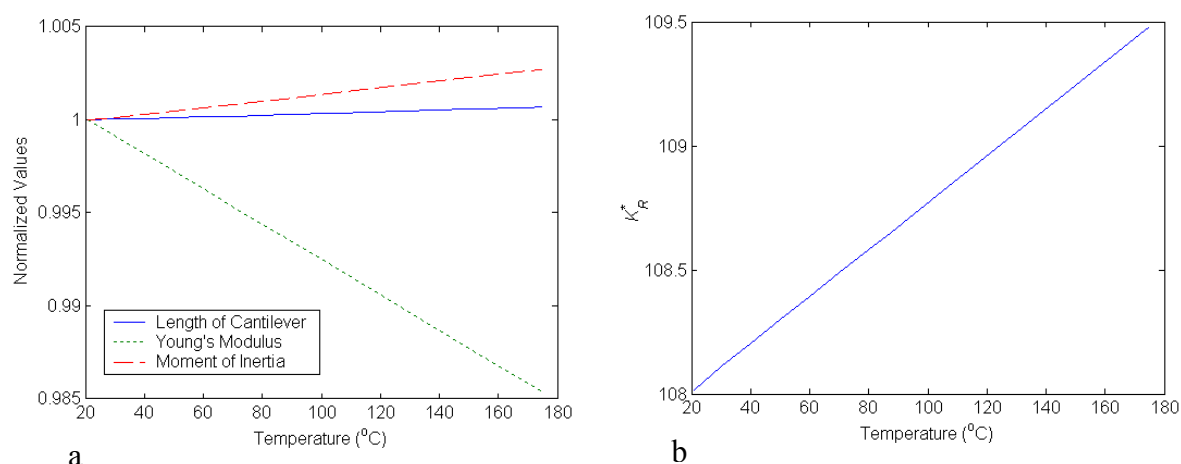


Figure 6. a) The normalized variation of length, Young's modulus of elasticity and moment of inertia for an AFM cantilever as a function of temperature. b) The change in the K_R^* value as a function of temperature.

Table 2. Electro-thermal dependence of the resonant frequency for the *G1* AFM cantilever. Experimental (*Exp*) and non-classical boundary (*NCB*) support theory.

T (°C)	<i>NCB</i>	<i>Exp</i>	<i>NCB</i>	<i>Exp</i>	<i>NCB</i>	<i>Exp</i>	<i>NCB</i>	<i>Exp</i>
	(Hz)	(Hz)	(Hz)	(Hz)	(Hz)	(Hz)	(Hz)	(Hz)
	<i>0V</i>	<i>0V</i>	<i>25V</i>	<i>25V</i>	<i>175V</i>	<i>175V</i>	<i>213.5V</i>	<i>213.5V</i>
21	10440	10440	10413	10424	8598	8608	5583	5615
30	10437	10434	10409	10420	8592	8601	5565	5605
40	10432	10430	10404	10415	8584	8593	5545	5581
50	10427	10424	10399	10410	8577	8585	5524	5558
60	10422	10421	10394	10406	8570	8577	5504	5534
70	10418	10418	10390	10400	8562	8569	5483	5511
80	10413	10414	10385	10396	8555	8561	5463	5487
87.5	10409	10410	10381	10393	8550	8555	5447	5469
105	10401	10401	10373	10384	8537	8541	5410	5426
150	10380	10382	10351	10363	8504	8504	5313	5313
170	10370	10373	10342	10354	8489	8488	5269	5262
175	10368	10370	10340	10351	8485	8484	5257	5249

The other AFM cantilevers, *G2-G12*, were further tested at room temperature using either an electrostatic AC sinusoidal base excitation or mechanical base excitation alone [40]. The electro-thermal independent resonant frequency obtained for each cantilever is presented in Table 3.

Table 3. The experimental (*Exp*) resonant frequencies (kHz) for the 12 geometries (*G*) tested and the rotational stiffness K_R^* values obtained to match the experimental values with the non-classical boundary support theory (tested at room temperature).

<i>G</i>	1	2	3	4	5	6	7	8	9	10	11	12
<i>Exp</i>	10.4	14.5	19.4	19.6	21.2	15.6	16.0	10.2	19.4	13.9	24.5	18.1
K_R^*	108	90	83	84	65.5	68	60	109	87	96	10.85	13.5

From the rotational stiffness values calculated in Table 3 it is not clear that the AFM cantilevers come from the same microfabrication process, hence they need to be quantified with respect to an effective rotational stiffness K_R^E given by,

$$K_R^E = \frac{K_R^{(T)*} E^{(T)} I^{(T)}}{L^{(T)}} \quad (1)$$

The non-dimensionalized rotational stiffness K_R^* and effective rotational stiffness K_R^E values obtained for the 12 AFM cantilevers tested are presented in Table 4. In this table, the geometries marked with an # are for AFM probes with a tip [29].

Table 4. A comparison of the rotational stiffness K_R^* and effective rotational stiffness K_R^E values for the 12 AFM cantilevers tested.

Indicates cantilevers with tip.

<i>AFM Probe</i>	K_R^*	K_R^E (N·m 10 ⁻⁹)
1	108	130.42
2	90	131.66
3 [#]	83	133.65
4 [#]	84	128.83
5 [#]	65.5	129.01
6 [#]	68	133.43
7 [#]	60	130.73
8 [#]	109	130.41
9 [#]	87	129.00
10 [#]	96	130.93
11 [#]	10.85	130.47
12 [#]	13.5	130.55

The results obtained for the individual AFM cantilever boundary supports clearly show the influence of microfabrication influences, as can be seen in the K_R^* values given in Table 4, where for a classical clamped support boundary K_R^* will have an infinitely high value. Furthermore, the effective rotational stiffness K_R^E values given in Table 4 are in very good agreement, with an average K_R^E value of 130.76×10^{-9} N·m resulting in standard deviation of 1.55×10^{-9} N·m for the experimental test results obtained, and in this regard, demonstrate the foundry influence in the microfabrication process. Hence, with this experimental approach, which is based on measuring the mechanical characteristics of a few AFM cantilevers under variant applied conditions, it is possible to extract the mechanical characteristics of similar devices manufactured using the same foundry microfabrication process. Furthermore, the experimental results obtained demonstrate the non-classical boundary support nature of AFM cantilevers due to microfabrication processes and limitations.

A comparison with 5 ideal nominal cantilevers is presented below. In this regard, the natural frequency results given in Table 3 are compared to the nominal values expected with the ideal geometry for each cantilever. The dimensions of the nominal cantilevers *NI-N5*, K_R^* values obtained using the experimentally obtained average K_R^E value of 130.76×10^{-9} N·m, and the respective natural frequencies are given in Table 5.

Table 5. Nominal cantilevers with ideal geometries. The associated tested cantilevers *G1-G12* are shown in parenthesis in the first column. The K_R^* values are obtained from the average K_R^E values obtained experimentally. The ideal natural frequency for each nominal cantilever is also given.

<i>Nominal Cantilever</i>	<i>L</i> (μ m)	<i>w</i> (μ m)	<i>h</i> (μ m)	K_R^*	K_R^E (N·m 10^{-9})	<i>Frequency</i> (Hz)
<i>N1</i> (<i>G2, G6, G7, G10</i>)	300	35	1	79.35	130.76	14940
<i>N2</i> (<i>G3, G4, G5, G9</i>)	250	35	1	66.13	130.76	21410
<i>N3</i> (<i>G11</i>)	300	35	2	9.92	130.76	25820
<i>N4</i> (<i>G12</i>)	350	35	2	11.57	130.76	19375
<i>N5</i> (<i>G1, G8</i>)	350	35	1	92.58	130.76	11014

For the cantilevers with the nominal *NI-N5* type geometry, respectively, the average difference in the natural frequency with respect to the nominal value is 5.4%, 7.1%, 5.1%, 6.6%, and 6.5%, respectively. This difference is due in part to the limitation in measuring the dimensions of each cantilever, and also to the resolution of the test equipment used for the experiments. In this regard, a geometry parameter defined as $\Gamma = \frac{wh^3}{L}$ is computed for each type of cantilever. This allows for a comparison of the effect of the measured geometries on the rotational stiffness K_R^* values obtained. Shown in Figure 7 are the normalized K_R^* values as a function of the normalized Γ parameter.

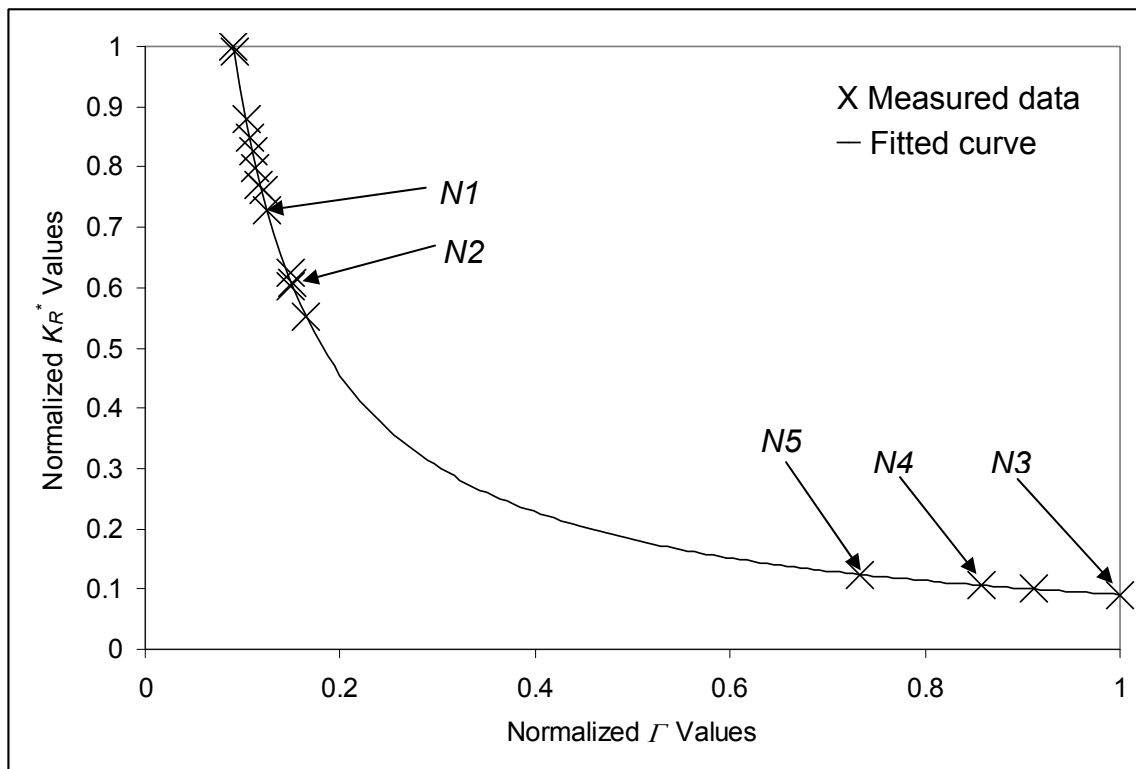


Figure 7. Calculated (from experiment and measured values) and fitted curve changes in the rotational stiffness K_R^* values as a function of the geometry of the cantilever. The values for the nominal ideal geometry cantilevers are pointed out.

It can be seen that the measured data fits very well with the fitted curve, as shown in Figure 7, from which it can be concluded that the experimentally obtained value of 130.76×10^{-9} N·m for the effective rotational stiffness K_R^E is valid for this microfabrication process. Also, it can be seen that the nominal geometry values also fit onto the curve which would suggest that even though small errors may have been introduced in measuring the dimensions of the cantilevers, they were not so great so as to make the measurements completely unreliable.

3. Conclusions

A quantitative experimental approach for the non-classical boundary characterization of AFM cantilevers by electro-thermal-mechanical testing has been presented. This approach allows for the extraction of mechanical properties of many different microcantilevers based on the mechanical characteristics of only a few cantilevers subjected to variant applied influences, and where all the devices tested were manufactured using the same microfabrication foundry process. This approach may be applied to other suspended MEMS structures and other microfabrication foundry processes. Support boundaries for suspended microstructures in general, are non-classical in nature and need to be evaluated experimentally. In this regard, the boundary support condition can be extracted from the effective rotational stiffness K_R^E values obtained through the frequency responses of the cantilevers obtained experimentally. These values are in very good agreement with the non-classical boundary support theory. Hence, for a given microfabrication process run, only one device need be tested under different operating conditions in order to obtain the mechanical characteristics of all the devices.

Although this method has been applied to a limited number of cantilevers fabricated using the same technology, it is expected that other microfabrication processes and limitations would have similar boundary support influences on the mechanical properties of the cantilever, resulting in an effective rotational stiffness for that particular microsystem foundry process. In this regard, future work in this area can be directed towards applying this method to other microfabrication technologies.

4. Experimental Section

A non-contact laser based optical method [40], was employed for the experimentation in this work as shown in Figure 8.

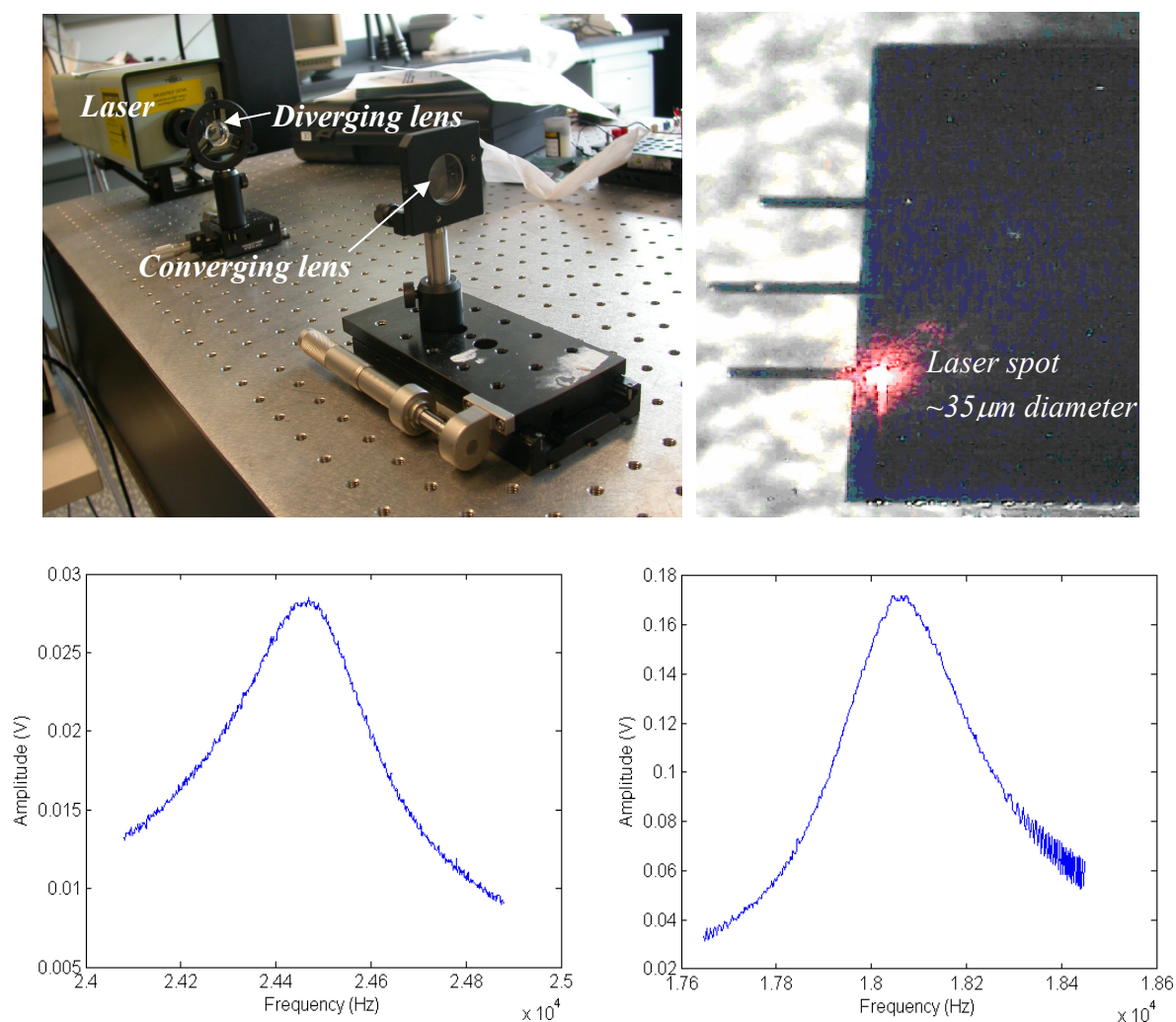


Figure 8. Top left: HeNe laser and lenses mounted on an optical bench. Top right: Digital image taken through a microscope of the laser spot on the AFM chip. Bottom: Sample responses obtained with the experimental method used in this work.

This approach brings significant versatility to the test environment in the sense that it allows one to readily incorporate electrostatic and thermal influences onto the microstructure platform which would otherwise be difficult in a confined environment. The base excitation for the AFM cantilevers was

provided by a small amplitude sinusoidal AC voltage or mechanical shaking using acoustic energy [40]. The frequency was swept (100-25 kHz) and a resonance response was obtained for the probe. The thermal loading [41] was applied with a MINCO [42] heating pad and regulator. Frequency measurements were taken at various applied DC voltage offsets and thermal loads. Shown in Figure 9 is a schematic overview of an electro-thermally activated AFM probe as used in this work.

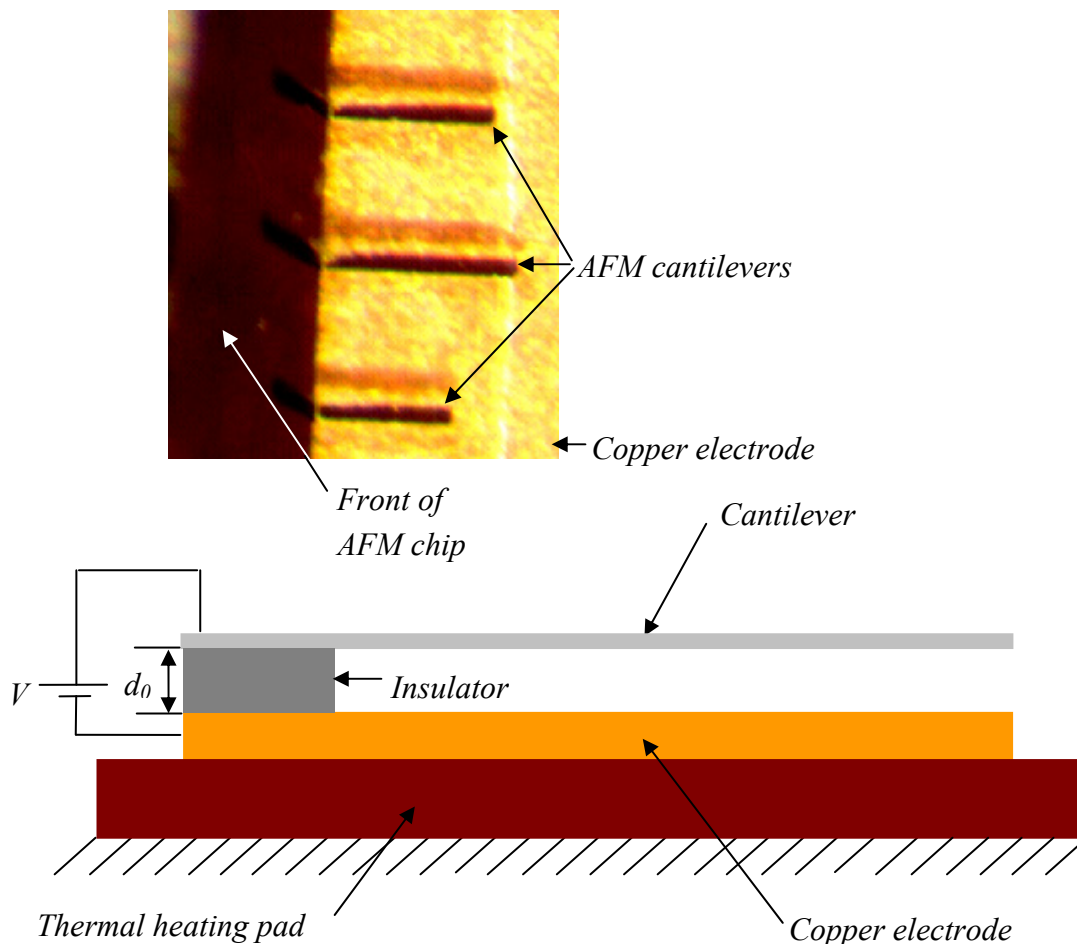


Figure 9. Top: Microscope image of an AFM chip and three AFM cantilevers.

Bottom: Schematic side view of a cantilever in an applied electro-thermal environment as carried out in this work.

The qualitative boundary support conditioning approach presented in this work consisted of testing one AFM cantilever ($G1$) under various electro-thermal loads and acquiring a support boundary characterization quantified through an invariant effective rotational stiffness K_R^E value. Eleven other cantilevers were also tested with the aim of obtaining an invariant boundary support condition quantified through an effective rotational stiffness K_R^E value that is independent of the device geometry (length, width and thickness) and that will quantify and define that particular foundry process. The approximated threshold voltage for the $G1$ AFM probe was ~ 225 V, hence, the applied DC offsets were limited to a maximum of ~ 215 V in order to accommodate any inaccuracies in the measurement of the dielectric gap (~ 51 μm).

In order to compare the experimental results with theoretical values, the Rayleigh-Ritz energy method is employed to model the dynamic electro-thermal system [17, 19, 26, 27, 29, 32]. This approach is a simple method to incorporate the combined effects of material properties, microfabrication influences and environment in the analysis of dynamic microsystems. The main advantage of this method over finite element methods is the time required to build the analytical model. The non-classical nature of the microsystem boundary support is modeled through the boundary support springs. The theoretical basis of the microcantilever starts with *free-free* boundary support conditions. In this formulation the boundary conditions can be modified through the boundary support springs, K_T^* and K_R^* . As there is no translational motion the value of K_T^* is maintained at a high value (1×10^{10}) so that at the very least *pinned-free* boundary conditions exist. The influence of K_R^* is then incorporated into the model to generate the “elastic” profile required to match the experimental natural frequency values obtained at various electro-thermal loads with the mathematical model. Hence, the non-classical nature of the boundary support is revealed through the K_R^E value obtained.

The high response of the fundamental frequency at resonance to a forced excitation makes it very suitable for analyzing the dynamic property of a vibrating system. In this regard, this method may be employed to estimate the natural frequencies of flexible structures such as AFM cantilevers. In this method the mechanical property of the system is a function of its potential and kinetic energies, and where the static (*S*) and dynamic (*F*) motion of the structure is estimated as,

$$D_{S,F}(x) = \sum_{i=1}^n A_i \Omega_i(x) \quad (2)$$

where D_S is used for the static deflection, and D_F is used for the flexural deflection of the AFM cantilever. The A_i are the deflection coefficients of the cantilever, $\Omega_i(x)$ are the orthogonal polynomials satisfying the geometrical boundary conditions, and x is a normalized coordinate equal to ξ/L .

The Rayleigh quotient is defined as,

$$\omega^2 = \frac{U_M}{T_M^*} \quad (3)$$

where,

$$T_M^* = \frac{T_M}{\omega^2} \quad (3a)$$

T_M is the maximum kinetic energy and U_M , is the maximum strain energy of the microstructure. In this regard, the maximum potential energy of the cantilever under electro-thermal mechanical influences is given by,

$$U^{(T)}_M = U^{(T)}_{AP} + U^{(T)}_{BSP} + U^{(T)}_E \quad (4)$$

where $U^{(T)}_{AP}$, $U^{(T)}_{BSP}$, and $U^{(T)}_E$ are the cantilever beam, boundary support springs and electrostatic potential energies, respectively. The superscript, (T) , indicates temperature and therefore, the thermal dependence of that particular variable.

The AFM probe portion of the maximum potential energy is given by,

$$U^{(T)}_{AP} = \frac{E^{(T)} w^{(T)} h^{(T)3}}{24L^{(T)3}} \int_0^1 (D_F''(x))^2 dx \quad (5)$$

the maximum kinetic energy is given by,

$$T_M^{(T)} = \omega^2 T_M^{*(T)} = \frac{1}{2} \omega^2 \rho^{(T)} w^{(T)} h^{(T)} L^{(T)} \int_0^1 (D_F(x))^2 dx \quad (6)$$

where the following definitions apply, $L^{(T)}$ is the length, $h^{(T)}$, is the thickness, $E^{(T)}$, is Young's modulus of elasticity, $\rho^{(T)}$ is the material density, $w^{(T)}$, is the width of the cantilever, $D_F''(x)$ is the second derivative of $D_F(x)$ with respect to x , and ω is the rotational frequency in rad/s.

The influence of the boundary support of the cantilever on the potential energy is given by,

$$U^{(T)}_{BSP} = \frac{1}{2} K_T (D_F(0))^2 + \frac{1}{2} \frac{K_R}{L^{(T)2}} (D_F'(0))^2 \quad (7)$$

where, $D_F(0)$ and $D_F'(0)$ are the deflection at the boundary support and the first derivative, respectively. By varying the values of K_R and K_T it is possible to vary the support boundary between a free and clamped condition. In the analysis presented here, only K_R^* is varied and K_T^* is maintained at a very high value due to the lack of translational motion. Hence, the microfabrication limitation at the support boundary of the AFM cantilever is quantified through the rotational stiffness.

The electrostatic potential energy, U_E , is derived from the static equilibrium position of the AFM cantilever, for a given electrostatic potential and thermal load. In this regard, an artificial electrostatic spring, $K_E^{(T)}$ [33], is introduced for a given electrostatic potential and thermal load. Starting with the electrostatic force variation given by,

$$F_E^{(T)}(x) = \frac{\epsilon_0 \epsilon_r w^{(T)} L^{(T)} V^2}{2} \left[\frac{1}{(d_0 - D_S(x))^2} \right] \quad (8)$$

where D_S is the static deflection of the probe for a given electrostatic potential and where the static equilibrium position is given by

$$P_S = d_0 - D_S(x) \quad (9)$$

the electrostatic stiffness variation, $k_E^{(T)}(x)$, is obtained from

$$k_E^{(T)}(x) = \frac{dF_E^{(T)}(x)}{dD_S(x)} = \varepsilon_0 \varepsilon_r w^{(T)} L^{(T)} V^2 \left[\frac{1}{(P_S)^3} \right] \quad (10)$$

and in normalized form,

$$k_E^{(T)*}(x) = \frac{\varepsilon_0 \varepsilon_r w^{(T)} L^{(T)4} V^2}{E^{(T)} I^{(T)}} \left[\frac{1}{(P_S)^3} \right] \quad (11)$$

where $I^{(T)}$ is the moment of inertia of the cantilever. The electrostatic potential energy, $U_E^{(T)}$, may then be obtained from,

$$U_E^{(T)} = \frac{1}{2} \int_0^1 k_E^{(T)*}(x) (D_F(x))^2 dx \quad (12)$$

The eigensystem defining the flexural deflection, D_F , of the cantilever for the condition [43],

$$\frac{\partial}{\partial A_i} [U_{AP}^{(T)} + U_{BSP}^{(T)} - U_E^{(T)} - T_B^{(T)}] = 0 \quad (13)$$

is given by,

$$\sum_j \left[H_{ij}^{22x} + K_T^{(T)*} H_{ij}^{000} + K_R^{(T)*} H_{ij}^{110} - K_E^{(T)*} H_{ij}^{00x} - \Lambda^{(T)} H_{ij}^{00x} \right] A_j = 0$$

$$\forall i = 1, 2, \dots, n \quad (14)$$

from which the eigenvalues, mode shapes and natural frequencies of the cantilever are obtained,

$$\Lambda_n^{(T)} = \lambda_n^{(T)2} = \frac{\omega_n^{(T)2} \rho^{(T)} h^{(T)} L^{(T)4}}{E^{(T)} I^{(T)}}, \quad \omega_n^{(T)} = \lambda_n^{(T)} \sqrt{\frac{E^{(T)} I^{(T)}}{\rho^{(T)} h^{(T)} L^{(T)4}}} \quad (15)$$

With respect to Equation (14), the following definitions apply,

$$H_{ij}^{22x} = \int_0^1 \Omega_i''(x) \Omega_j''(x) dx \quad (16)$$

$$H_{ij}^{00x} = \int_0^1 \Omega_i(x) \Omega_j(x) dx \quad (17)$$

$$H_{ij}^{000} = \Omega_i(0) \Omega_j(0) \quad (18)$$

$$H_{ij}^{110} = \Omega_i'(0) \Omega_j'(0) \quad (19)$$

$$K_T^{(T)*} = \frac{K_T^E L^{(T)3}}{E^{(T)} I^{(T)}}, \quad K_R^{(T)*} = \frac{K_R^E L^{(T)}}{E^{(T)} I^{(T)}} \quad (20)$$

The eigenvalues and mode shapes given by Equation (14) will be a fundamental indicator of the mechanical characteristics of the AFM cantilever, and in this regard, the support boundary conditions. Illustrated in Figure 10 is the dependence of the first and second eigenvalues on the rotational stiffness K_R^* .

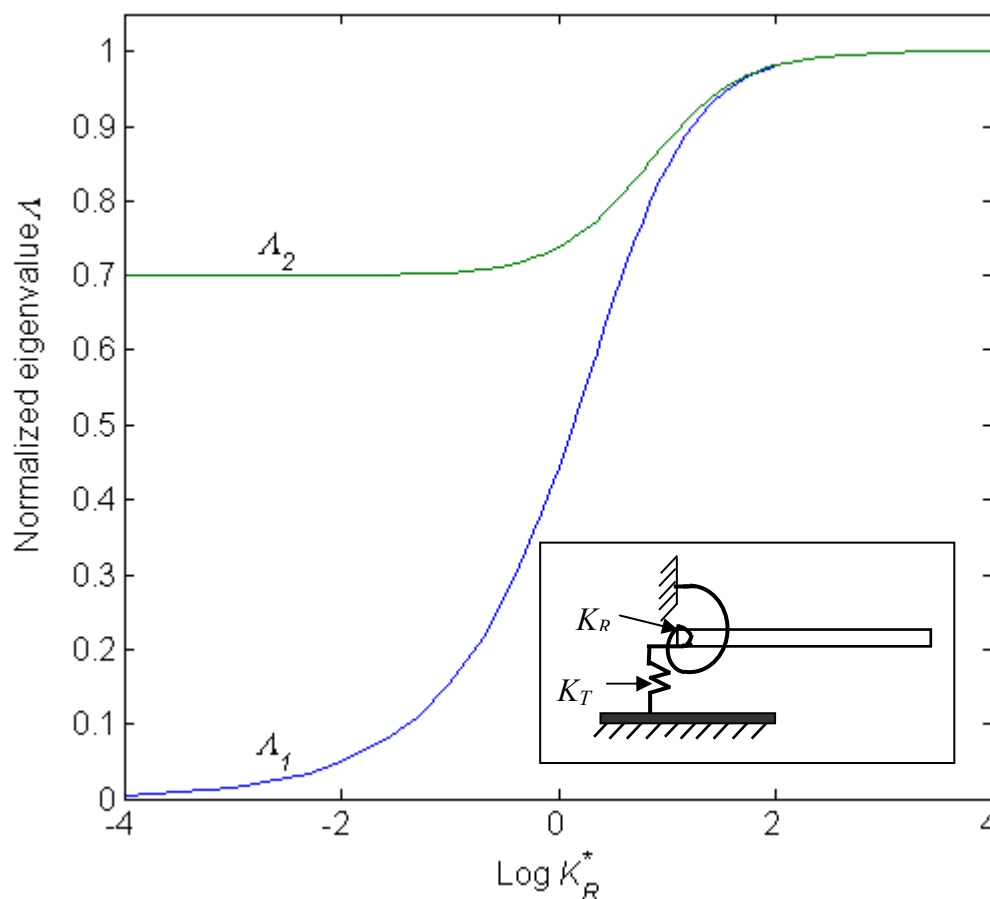


Figure 10. The variation of the first and second normalized eigenvalues of a boundary supported structure as a function of the rotational stiffness K_R^* .

References and Notes

1. Thundat, T.; Oden, P.I.; Warmack, R.J. Chemical, Physical, and Biological Detection using Microcantilevers. In Proceedings of the Third International Symposium on Microstructures and Microfabricated Systems, 1997; 179-187.
2. Raiteri, R.; Grattarola, M.; Butt, H.J.; Skladal, P. Micromechanical Cantilever-Based Biosensors. *Sensors and Actuators B* **2001**, *79*, 115-126.
3. Brown, K.B.; Allegretto, W.; Vermeulen, F.E.; Robinson, A.M. Simple Resonating Microstructures for Gas Pressure Measurement. *Journal of Micromechanics and Microengineering* **2002**, *12*, 204-210.
4. Su, M.; Li, S.; Dravid, V.P. Microcantilever Resonance-Based DNA Detection with Nanoparticle Probes. *Biochemical and Biophysical Research Communications* **2003**, *304*, 98-100.
5. Fadel, L.; Dufour, I.; Lochon, F.; Français, O. Signal-to-Noise Ratio of Resonant Microcantilever Type Chemical Sensors as a Function of Resonant Frequency and Quality Factor. *Sensors and Actuators* **2004**, *102*, 73-77.
6. McFarland, A.W.; Colton, J.S. Chemical Sensing with Micromolded Plastic Microcantilevers. *Journal of Microelectromechanical Systems* **2005**, *14*, 1375-1385.
7. Huang, R.S.; Abbaspour-Sani, E.; Kwok, C.Y. A Novel Accelerometer Using Silicon Micromachined Cantilever Supported Optical Grid and PIN Photodetector. In Proceedings of the 8th International Conference on Solid-State Sensors and Actuators, 1995, 663-666.
8. Burchman, K.E.; Boyd, J.T. Freestanding, Micromachined, Multimode Silicon Optical Waveguides at $\lambda = 1.3\mu\text{m}$ for Microelectromechanical Systems Technology. *Applied Optic.* **1998**, *37*, 8397-8399.
9. Wang, W.-C.; Fauver, M.; Nhut Ho, J.; Seibel, E.J.; Reinhall, P.G. Development of an Optical Waveguide Cantilever Scanner. in *Proceedings of SPIE, Opto-Ireland: Optics and Photonics Technologies and Applications* **2002**, 72-83.
10. Dragoman, D.; Dragoman, M. Biased Micromechanical Cantilever Arrays as Optical Image Memory. *Applied Optics* **2003**, *8*, 1515-1519.
11. Manalis, S.R.; Minne, S.C.; Atalar, A.; Quate, C.F. Interdigital Cantilevers for Atomic Force Microscopy. *Applied Physics Letters* **1996**, *69*, 3944-3946.
12. Pedersen, N.L. Design of Cantilever Probes for Atomic Force Microscopy (AFM). *Engineering Optimization* **2000**, *32*, 373-392.
13. Kawakatsu, H.; Saya, D.; Kato, A.; Fukushima, K.; Toshiyoshi, H.; Fujita, H. Millions of Cantilevers for Atomic Force Microscopy. *Review of Scientific Instruments* **2002**, *73*, 1188-1192.
14. Brook, A.J.; Bending, S.J.; Pinto, J.; Oral, A.; Ritchie, D.; Beere, H.; Springthorpe, A.; Henini, M. Micromachined III-V Cantilevers for AFM Tracking Scanning Hall Microscopy. *Journal of Micromechanics and Microengineering* **2003**, *13*, 124-128.
15. Lee, D.-W.; Wetzels, A.; Bennewitz, R.; Meyer, E.; Despont, M.; Vettiger, P.; Gerber, C. Switchable Cantilever for a Time-of-Flight Scanning Force Microscope. *Applied Physics Letters* **2004**, *84*, 1558-1560.

16. Mullen, R.; Mehregany, M.; Omar, M.; Ko, W. Theoretical Modeling of Boundary Conditions in Microfabricated Beams. in *Proceedings of IEEE Micro Electro Mechanical Systems, Conference on Micro Structures, Sensors, Actuators, Machines and Robots* **1991**, 154-159.
17. Rinaldi, G.; Packirisamy, M.; Stiharu, I. An Improved Method for Predicting Microfabrication Influence in Atomic Force Microscopy Performances. *International Journal of Nanotechnology* **2004**, *1*, 292-306.
18. Packirisamy, M.; Stiharu, I.; Bhat, R.B. Influence of Micromachining on Dynamic Behavior of MEMS Structures. *Canadian Journal of Electrical and Computer Engineering* **2005**, *30*, 157-162.
19. Rinaldi, G.; Packirisamy, M.; Stiharu, I. Multiparameter Synthesis of Microsystems. in *Proceedings of SPIE, International Conference on Photonic Devices* **2005**, 5970, 333-344.
20. Howe, R. Surface Micromachining for Microsensors and Microactuators. *Journal of Vacuum Science and Technology* **1988**, *6*, 1809-1813.
21. Delapierre, G. Micromachining: A Survey of the Most Commonly used Processes. *Sensors and Actuators B* **1989**, *17*, 123-138.
22. Benitez, M.A.; Plaza, J.A.; Sheng, S.Q.; Esteve, J. A New Process for Releasing Micromechanical Structures in Surface Micromachining. *Journal of Micromechanics and Microengineering* **1996**, *6*, 36-39.
23. Madou, M. in *Fundamentals of Microfabrication*. CRC Press LLC, Boca Raton, 1997, p. 56.
24. Kovacs, G.T.A.; Maluf, N.I.; Petersen, K.E. Bulk Micromachining of Silicon. in *Proceedings of the IEEE* **1998**, *86*, 1536-1551.
25. Judy, J.W. MicroElectroMechanical Systems (MEMS): Fabrication, Design and Applications. *Smart Materials and Structures* **2001**, *10*, 1115-1134.
26. Packirisamy, M.; Stiharu, I.; Bhat, R.B. Application of Boundary Conditioning to the Synthesis of Microsystems. in *Proceedings of the Micro Electro Mechanical Systems Conference* 2001, 83-86.
27. Packirisamy, M.; Bhat, R.B.; Stiharu, I. Boundary Conditioning Technique for Structural Tuning. *Journal of Sound and Vibration* **1999**, *220*, 847-859.
28. Rinaldi, G.; Packirisamy, M.; Stiharu, I. Experimental Investigation on the Dynamics of MEMS Structures. in *Proceedings of SPIE, International Conference on MEMS, MOEMS and Micromachining* **2004**, 5455, 66-73.
29. Rinaldi, G.; Packirisamy, M.; Stiharu, I. Boundary Characterization of Microstructures through Thermo-Mechanical Testing. *Journal of Micromechanics and Microengineering* **2006**, *16*, 549-556.
30. Ollier, E. Optical MEMS Devices based on Moving Waveguides. *IEEE Journal on Selected Topics in Quantum Electronics* **2002**, *8*, 155-162.
31. MikroMasch Technical Data Sheet, 2002: CSC38/AIBS/15. www.spmtips.com.
32. Bhat, R.B. Natural Frequencies of Rectangular Plates using Characteristic Orthogonal Polynomials in Rayleigh-Ritz Method. *Journal of Sound and Vibration* **1985**, *102*, 493-499.
33. Rinaldi, G.; Packirisamy, M.; Stiharu, I. Electrostatic Boundary Conditioning of MEMS Devices. in *Proceedings of the 8th International Cairo University MDP, Conference on Current Advances in Mechanical Design and Production VIII* **2004**, 269-276.

34. Roberts, R.B. Thermal Expansion Reference Data: Silicon 300-850 K. *Journal of Physics D: Applied Physics* **1981**, *14*, 163-166.
35. Okaji, M.; Imai, H. A Practical Measurement System for the Accurate Determination of Linear Thermal Expansion Coefficients. *Journal of Physics E: Scientific Instrument* **1984**, *17*, 669-673.
36. Ono, N.; Kitamura, K.; Nakajima, K.; Shimanuki, Y. Measurement of Young's Modulus of Silicon Single Crystal at High Temperature and Its Dependency on Boron Concentration Using the Flexural Vibration Method. *Japanese Journal of Applied Physics* **2000**, *39*, 368-371.
37. Glazov, V.M.; Pashinkin, A.S. The Thermal Properties (Heat Capacity and Thermal Expansion) of Single-Crystal Silicon *High Temperature* **2001**, *39*, 413-419.
38. Han, J.; Zhu, C.; Liu, J.; He, Y. Dependence of the Resonance Frequency of Thermally Excited Microcantilever Resonators on Temperature. *Sensors and Actuators* **2002**, *101*, 37-41.
39. Watanabe, H.; Yamada, N.; Okaji, M. Linear Thermal Expansion Coefficient of Silicon from 293 to 1000 K. *International Journal of Thermophysics* **2004**, *25*, 221-236.
40. Rinaldi, G.; Packirisamy, M.; Stiharu, I. Dynamic Testing of Micromechanical Structures under Thermo-Electro-Mechanical Influences. *Measurement* **2006**, Accepted Manuscript.
41. Rinaldi, G.; Packirisamy, M.; Stiharu, I. Optical MEMS Based Bimorph for Thermal Sensing. in *Proceedings of SPIE, Symposium on Canadian and International Business and Technology Innovations in Optics and Photonics* **2004**, *5577*, 628-635.
42. Bulletin: TS-103(A), July 2004, MINCO Products Inc., Minneapolis, MN, USA.
43. Bhat, R.B. Nature of Stationarity of the Natural Frequencies at the Natural Modes in the Rayleigh-Ritz Method. *Journal of Sound and Vibration* **1997**, *203*, 251-263.